THROUGH THICKNESS LASER JOINING OF CONTINUOUS GLASS FIBER FABRIC REINFORCEMENT

Paper Number 405

Huade Tan, Gen Satoh, Y. Lawrence Yao

Manufacturing Research Laboratory
Department of Mechanical Engineering Columbia University, New York, New York, 10027, USA

Abstract

Inter laminar crack initiation and propagation is a major failure mode in structural composite applications. Manufacturing induced fiber discontinuities within a laminate composite act as stress concentrations and initiation sites of such delamination cracks. A local inter laminar reinforcement method is proposed to mitigate the effects of manufacturing induced stress concentrations and increase the local fracture toughness of the composite. A through thickness laser fusion joining process is developed for the out of plane reinforcement of glass fiber pre-forms used in the vacuum infusion fabrication of thick composite structures. Laser joining is achieved through a thermal fusion process which joins fibers within a single bundle and fiber bundles between successive woven fabric layers. Coupled two phase heat transfer and viscous flow modeling is carried out to simulate the temperature and morphology of the joining process under experimentally observed conditions. Mode I fracture toughness of through thickness reinforced composite laminates is measured experimentally and compared to un-reinforced plane weave glass composites. Laser fusion joint effects on mode I crack propagation and fracture dynamics are observed through high resolution imaging during the crack propagation process and post mortem imaging of the fracture surface. Increased delamination resistance of laser joined composites is found to be a function of the joint thickness.

Introduction

Fiber placement and resin infusion processes determine the final form and function of a polymer matrix composite part. Reinforcement architecture is the determining factor in the composite's mechanical properties. The ideal reinforcement architecture of a composite under multi axial loading is often not unidirectional. The objective of this work is to develop a novel manufacturing process in the fabrication of composites: to improve the out of plane strength and to allow greater flexibility in the design and application of such materials.

Manufacturing of continuous fiber polymer matrix composites primarily consist of either pre-impregnation (pre-preg) or transfer molding (pre-form) processes. Pre-preg composite fabrication consists of placing densely packed resin infused tapes of reinforcement fibers in layers (laminates) to produce thin shell structures. Composites manufactured from pre-preg processes exhibit high fiber packing fraction and high strength along the fiber directions. Pre-preg fabricated composites exhibit low strength in the inter laminar direction because they contain no fiber reinforcements through thickness due to the layer by layer assembly process. Pre-preg fabrication is undesirable for composites requiring high through thickness strength and fracture toughness. Through thickness strength has been shown to increase with the insertion of metal pins (z-pins) through layers of pre-preg prior to curing [1]. Through thickness strength is improved by z-pins from matrix load transfer mechanisms between the fibers and pins. Z-pinning has been shown to be undesirable in some cases because the insertion of pins displaces fibers in the lamina and introduces pockets of resin rich regions which act as stress concentrations, resulting in reduced planar strength.

Composites manufactured from fiber pre-forms involve the assembly of fiber bundles into near form structures which are later infused and cured using a vacuum assisted or other such resin infusion process. Resin transfer molding of woven fiber pre-forms have been shown to produce composites with desirable fiber packing and through thickness strength. Through thickness strength is achieved by distributing reinforcement fibers in the thickness direction using various stitching and weaving techniques [2,3]. The introduction of woven fibers or stitching materials in the thickness direction, however, also displaces fibers in the planar directions, similar to pinning. Woven pre-forms have been shown to yield significant improvements in out of plane material properties [4].

Woven three dimensional fiber reinforcement pre-forms have been implemented in the production of thick composite parts with improved through thickness strength [3,4]. In addition to improved mechanical properties, three dimensional woven pre-forms have

been shown to improve fiber placement accuracy and reduce lay-up costs. A major process complication of 3d woven pre-form fabrication, however, is the cost and complexity of the machinery required in the weaving process. The fiber architecture of a 3d woven pre-form is dictated by complex 3d looms [4]. A 3d woven pre-form composite of non constant thickness or irregular geometry requires expensive loom set ups or secondary machining after resin infusion and curing, adding to the cost of the process and impairing the strength of the material. A comparable process to 3d weaving with a lower upfront cost and greater manufacturing flexibility is desirable.

Laser fusion joining, depicted in Figure 1, presents potential advantages in strength over stitching, weaving or adhesion methods in its high reinforcement density and direct fiber to fiber joining in the through thickness direction. Laser processing allows joints to be restricted to highly localized regions, i.e. regions of existing stress concentrations. Laser fiber joining requires a lower upfront cost and allows for greater flexibility in part geometry and fiber architecture than 3d weaving processes. Computer controlled manipulation and processing using laser irradiation to concurrently cut and join textiles reduces material waste and improves inventory efficiency. High weld rates may be achieved with existing laser and optics technologies.

A challenge in the fusion joining of woven fibers, as observed in textile joining investigations [5,6], is the tendency of the melt pool to flow away from the desired joint region, forming voids in the processing zone. Woven textiles and composite pre-forms are composed of many bundles of fibers, each of which is composed of hundreds of individual fibers. Fiber fusion and compaction processes during joining [7] causes significant local strains due to compaction because the relative density of a fused joint is much greater than that of the initial fiber bundle. The total volume of a fiber bundle required to form a joint is greater than the volume of the joint. During the fusion process, compaction and capillarity effects between the melt and the fiber bundle drive bulk flows of the melt away from the center of the joint toward the low density regions of the unprocessed fiber bundle. What results is the undesirable formation of voids, leading to poor load transfer and poor strength across the joint. In order to achieve fusion joining of 3d fiber pre-forms, we investigate the technical challenges inherent in the fiber fusion process.

A through thickness joining process for glass fiber reinforcement pre-forms is developed which overcomes the relative density and flow induced void formation problem. The process compensates for the compaction and flow behavior of the fiber bundle during fusion and achieves dense joints composed of glass reinforcement material. Numerical solutions using a two phase temperature dependent viscous flow model are shown to reproduce the melt flow pattern and joint morphology during a through thickness fusion joining process. Mode one fracture toughness testing of fusion joined samples is performed. Toughening effects introduced by inter laminar joining is studied to evaluate the strengthening mechanism of through thickness laser joining. Scanning electron microscopy is used to study the crack blunting and deflection effects on the fracture surface of joined samples.

Experimental Setup

Laser fusion joining and fabrication of woven glass reinforced composites is proposed as an intermediate process taking place during the fiber lay-up process. Prior to applying the resin matrix material, a stack of woven fiber reinforcements are fused together using localized laser energy. The stack of woven fabric is then sealed and prepared for vacuum assisted resin transfer molding (VARTM), where the matrix material is infused into the entire stack of fibers and allowed to cure. Cured composite panels sized six inches by eight inches are cut into one inch by seven inch beams following the ASTM standard D5528 [8] for fracture toughness testing. Each panel contains four samples, consisting of fiber fabrics that had been joined in the mid plane. Joint thicknesses of four and eight woven layers were fabricated and tested in this method. Joint and fiber fracture surfaces were imaged using SEM after mechanical tests to evaluate the crack propagation process during mode one delamination. Fracture surfaces of the joint and fiber structure were compared with mechanical testing results to understand the strengthening and fracture toughness enhancement mechanism.

Through thickness laser joining

Laser joining of e-glass fibers was achieved using an Nd:YAG laser operating at a constant 30W. All glass samples consist of 99.98% E-glass plain weave fabric. Samples were prepared from six ounce per yard plain woven fabric with 18 bundles of fiber per inch and 300 fibers per bundle. The Gaussian laser spot was focused to 0.8mm using a final objective with a numerical aperture of 0.26. Joint placement and motion control was accomplished using a six axis robotic manipulator with a flat sample holder.

E-glass is highly transmitting at near infrared (1064 nm). It is observed that densely packed E-glass fibers

are of sufficient opacity to initiate heat accumulation and flow. Infrared absorption of highly transmitting materials due to multiple surface scattering has previously been observed in investigations of densely packed beds of glass spheres [9] and porous media [10]. Absorption of glass is also known to be highly dependent on temperature [11]. Glass simultaneously absorbs and emits a wide range of wavelengths near the phase transition temperature [12,13].

Although other laser textile applications have evaluated the use of absorptive coatings for heat accumulation, it was determined from initial irradiation trials that surface coatings induce uneven absorption and poor joint density. Chemical decomposition and oxidation occurs in fibers with surfacing agents owing to the localized heating and the dramatic increase in laser absorption at elevated temperatures [13]. Temperature becomes uncontrollable once oxidation and vaporization initiates. If the melt pool is allowed to exceed the vaporization temperature, ionization quickly follows, and the resulting plasma consumes the entire melt pool and any surrounding fiber material within the spot radius. Uniform thermal absorption within the target spot is desired.

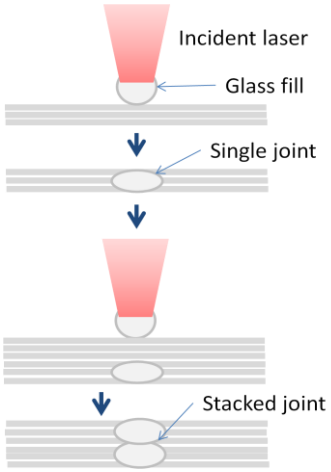

Figure 1: Inter laminar joining process schematic showing the layered building process of laser fusion joining. Each joint is aligned with the joint below it to form a continuous stack of joints in the through thickness.

The dominant material transport process for glass fusion and densification processes is viscous flow and capillarity, as cited in glass sintering processes [14,15]. As the melt volume increases, gravitational force becomes significant compared to the capillary and viscous forces. A particular challenge to fusion joining of fibrous systems is the high surface area and low relative density of the initial material. The joining method devised in this work, depicted in Figure 1, derives from the need to accommodate for viscous flow effects inherent in the fiber system.

Joint Enhanced Fracture Toughness Measurement

After laser joining, woven fabric reinforcements were infused with system 2000 epoxy resin from Fibreglast industries with a vacuum assisted resin transfer molding method (VARTM). Six inch by eight inch panels 32 layers thick (5mm) were cut and fabricated into double cantilever beam samples as described by ASTM D5528. Samples were joined in the mid plane of the beam where the crack initiation layer is placed into the specimen. Joints were placed on the beam's central axis at 10mm intervals along the length of the beam as depicted in Figure 9.

Samples were tested under displacement control using an Instron material testing system (MTS). Samples were tested at a constant 5mm per minute cross head speed without unloading after crack initiation. Various loading rates were evaluated during initial trials, with 5mm per minute selected to minimize the effect of plasticity ahead of the crack tip [16]. Cross head extension data is collected from the MTS machine's linear actuator and load is collected by a 2kN load cell with 0.01 Newton precision. A synchronized data acquisition system was used to capture an image of the crack front at every 1mm of cross head displacement and simultaneously record the extension and load. Mode one fracture energy release rate is calculated from the Modified Compliance Calibration method using the equation

$$G_I = \frac{3P^2C^{\frac{2}{3}}}{2A_1bh}, \qquad (1)$$

where P is the load recorded, b is the beam width, h is the beam thickness, $C = \frac{\delta}{P}$ is the compliance of the beam, δ is the extension of the sample and A_1 is the slope of the least squares regression of the thickness normalized crack length as a function of the cubed root of compliance.

Load versus displacement, load versus crack length and delamination resistance results obtained from DCB experiments are studied to characterize the fracture toughness along the crack plane on a spatially resolved scale. A 1mm cross head displacement interval between data points is of sufficient spatial resolution to capture the significantly varying fracture toughness between joined and the non-joined regions within the sample. High spatial resolution data obtained with this method yields added insight into the fracture

propagation process and allows for the decoupled analysis of laminate and joint fracture.

Numerical Simulation

A two dimensional two phase fluid heat transfer compressible flow model is implemented to simulate the flow behavior of the molten pool during fiber joining. The simulation concurrently solves the compressible Navier Stokes equations for viscous fluid flow, phase field (Cahn Hilliard) equations for two phase immiscibility and velocity dependent heat equations, as described in a previous paper [17]. Phase, density and temperature evolution output from the multi physics model yield spatially resolved time dependent flow of glass with and without the addition of fill material. Laser heat input is assumed to be a Gaussian distribution in the radial and constant in the z direction. The laser power density is calculated from the total power input into the material over the laser interaction volume. An absorption fraction α is used to adjust the simulation output by matching the temperature profile of the melt pool to that of molten glass during joining. The laser energy is applied only in the glass phase of the simulation domain.

As glass softens, the flow rate of the glass phase is captured by the temperature dependent viscosity in the Vogel-Fulcher-Tammann equation: given for E-glass as [18]

$$\eta(\mathrm{T}) = 10^{-4.88+\frac{6227}{T-268}}, \qquad (2)$$

where η is the glass dynamic viscosity ($Pa * s$) and T is the glass temperature in degrees Celsius. It is due to this highly temperature dependent viscosity that the single glass fluid phase behaves both as a solid and a fluid during the simulation. The dynamic viscosity of E-glass decreases by eight orders of magnitude in the glass transition range between 700 and 1400 degrees Centigrade. The dramatic reduction in viscosity of glass dictates much of the physical response of the material during joining.

Fiber compaction is modeled after the continuous media theory of selective laser sintering presented by Kolossov et. al. [19], where the degree of fiber densification is defined by a monotonically increasing sintering potential ϕ given by

$$\phi(\boldsymbol{x}, t) = 1 - e^{-\int_0^t \zeta(T(\boldsymbol{x},s))ds}, \qquad (3)$$

where ϕ is a continuous variable [0,1) corresponding to either separate fibers at $\phi = 0$ or fully dense glass at $\phi = 1$. The compaction rate $\zeta(T)$ is the rate of densification is first derived by Frenkel and later expanded upon by many authors [20–22] to be a temperature dependent function given by

$$\zeta = \frac{\gamma}{\eta(T) d_0}, \qquad (4)$$

where γ is the surface energy, $\eta(T)$ is the viscosity and d_0 is a characteristic length scale of the initial material. Neither the surface tension $\left[200 - 400 \frac{mJ}{m^2}\right]$ nor characteristic length of glass fiber ($10\mu m$) is highly dependent upon temperature relative to its viscosity. The densification rate of glass fiber may thus be reduced to a function of glass viscosity

$$\zeta(T) = k \frac{1}{\eta(T)}. \qquad (5)$$

Viscosity and compaction rates of E-glass and soda lime glass are plotted as a function of temperature in Fig. [1].

The conductivity of partly dense material is defined in Kolossov's model as

$$k_\phi = (a + (b - a)\phi) k_{bulk}, \qquad (6)$$

where $0 < a < 1$ and $0 < b \leq 1$ are the ratios of conductivity between loose fibers and densely packed fibers to the bulk such that $a \ll b$. Bulk thermal conductivity of glass is observed to be relatively constant with respect to temperature in the glass transition range [23]. At sufficient temperatures, glass spontaneously emits and absorbs infrared radiation, leading to a temperature dependent radiation factor in the thermal conductivity of the glass phase is given by

$$k_{rad}(\mathrm{T}) = \frac{16 n^2 \sigma T^3}{3\gamma}, \qquad (7)$$

where n is the refractive index of glass, σ is the Stefan-Boltzmann constant, and γ is a geometric parameter relating to the absorption over the mean free path of the material [24,25]. Because fibers are anisotropic and oriented only in the planar directions, the material conductivity is assumed to be

$$k_i = (a_i + (b - a_i)\phi)(k_{bulk} + k_{rad}), \qquad (8)$$

where the initial conductivity ratio in the a_x and a_y directions are assumed to be 0.01 and 0.1 respectively and b is assumed to be 1.

The model is bounded in a semi-infinite domain with a single horizontal parting line separating the initial volume fraction domains of air and glass phases. Simulations of the joining process include a spherical bead located directly above the phase separation boundary. The initial condition of the

density potential is taken to be $\phi = 1$ within the bead and $\phi = 0$ everywhere else. No slip and constant temperature boundary conditions are applied at the perimeter of the solution domain. The boundary of the fluid domain is set to zero velocity along the outer boundary of the glass phase and zero pressure along the boundary of the air phase such that the total mass of glass is conserved during the simulation.

Results and Discussion

Laser fusion joining of multiple layers of woven glass fiber fabrics is possible when a solid glass filler material is introduced at the laser focus in order to overcome the densification and flow effects observed during localized heating of woven glass fabrics. Joint morphology and penetration was measured experimentally and a numerical model has been implemented to capture the physical effects of viscous densification during the joining process. Strength and fracture toughness enhancement of the laser processed composite has been measured experimentally from double cantilever testing of woven fabric composites joined in the mid plane. Delamination resistance has been shown to be a function of the joint thickness.

Fiber Compaction Morphology

Laser irradiation of woven fiber mats generates rapid consolidation of fibers at the laser focal point. Fibers approaching the transition temperature of E-glass shorten and agglomerate to its nearest neighbor, forming pockets of dense glass at the focus. Anisotropic shrinkage and wetting of the molten glass into the surrounding fiber materials causes the material at the center of the focus to flow outward. The resulting morphology of the melt is a ring of solid glass around the focal volume, as depicted in Figure 2.

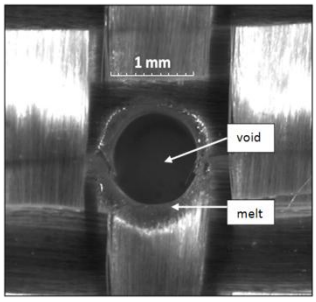

Figure 2: Optical micrograph of the surface fiber morphology after laser irradiation of a single layer of plane woven fabric. A dense ring of glass is formed during the heat induced compaction of fibers within the fabric.

The dynamics of melt formation and separation of woven fabric has been studied experimentally and plotted in Figure 3. During the compaction process, molten glass flow is observed to increase monotonically in both diameter and depth as a function of exposure time. The diameter of the melt pool is found to increase rapidly and decay to a maximum diameter of approximately 1mm, slightly larger than the laser spot size. The depth of the melt pool is found to increase linearly in time with no apparent maximum within the range of exposure times evaluated in this study. The melt flow dynamics observed in this work is thought to be resultant from the laser energy input and the fluid flow behavior of the fiber substrate.

Laser energy absorption is highly dependent upon the multiple scattering effects of the inhomogeneous glass fiber media. As low viscosity glass compacts and flows away from the center of the laser focus, incoming laser energy penetrates through the layer and is not absorbed. At a sufficient melt diameter, a self limiting state exists where the heat input into the material is such that the fiber surface tension is in equilibrium with the viscous flow resistance and a static equilibrium is reached in the radial direction.

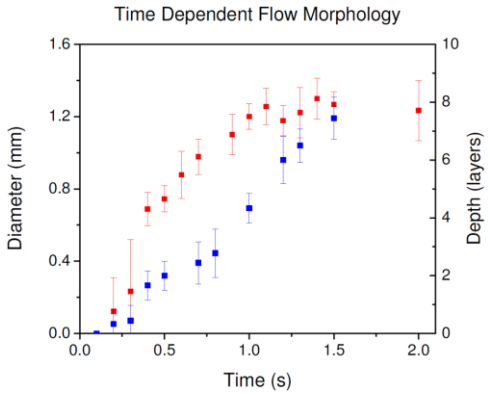

Figure 3: Measurements from optical micrographs of the morphological evolution of an in depth joint as a function of time. Note that the diameter of the melt ring reaches a steady state and plateaus while the depth of laser penetration is observed to be approximately linear up to the maximum thickness tested.

As molten glass flows away from the focal point, laser radiation passes deeper into the material and the process is repeated in each successive layer. The laser penetration progresses linearly during the melt separation process as is observed in Figure 3. As glass melt separates in the layer above, the layer below receives ever increasing energy and therefore begins to melt before the maximum diameter is reached in the layer above. Given a collimated laser beam with low dispersion, the melt morphology of the fabric is

expected to be constant in diameter with respect to depth. A focused laser was used in this experiment with a numerical aperture of 0.26, causing the beam to diverge away from focus. Beam divergence is expected to cause non constant melt diameter in depth and result in a maximum depth beyond which the laser intensity is insufficient to initiate fiber fusion. Within the depth of joints evaluated in this study, there was no detectable effect of laser dispersion on the penetration dynamics.

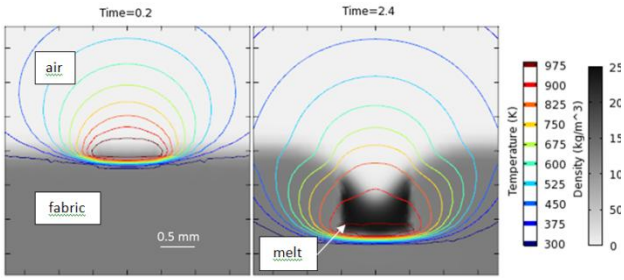

Figure 4: Numerical output of the glass densification process without filler material. The substrate is shown to form a void in the center of the laser focus with the maximum temperature at the base of the laser penetration depth.

Coupled laser heating, densification and flow dynamics are captured in the transient multi physics scheme, with a stationary heat source input into a continuous substrate without any fill. Fiber melt morphology, as depicted by the area of fully dense glass, and glass temperature obtained from the simulation are depicted in Figure 4.

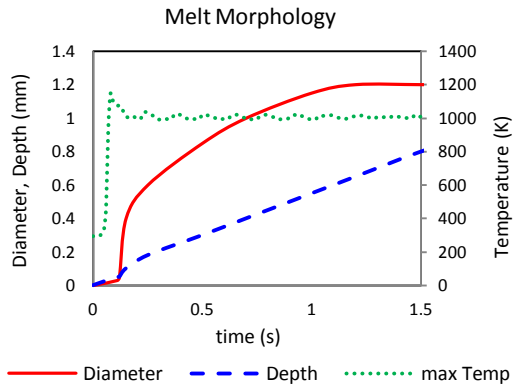

Figure 5: Numerical output of the time dependent joint morphology: temperature depth and diameter as a function of time. The melt diameter and depth is shown to follow the same trend as the experiments observed under optical microscopy.

The temperature profile and maximum temperature is observed to reach a steady state in time as the melt absorption and temperature gradient reaches a balance with the flow field as depicted in Figure 5. From these results, it is apparent that the melt morphology is closely linked to the temperature field of the solution, as is dictated by the temperature dependent densification function. It is also observed that for a stationary laser heat source, the temperature and diameter of the melt reaches a maximum, as has been confirmed from experiments. The material flow field and densification pattern depicted in Figure 4 is shown to match that observed from morphological studies. Morphology and dynamics agreements between the model and experiments give good confidence in the multi physics model for the prediction of melt morphologies in the fill assisted joining process.

Joint Morphology

The formation of a dense joint between multiple fabric layers is achieved when laser irradiation is coupled to the fabric through a solid fill material. Solid glass fill in the form of soda lime glass beads serves two functions in the joining process: to facilitate laser energy penetration into the fabric and to replace the fabric material as it flows away from laser heat source. During the fill induced joining process, laser energy is absorbed in the fibrous material and conducted into the fill bead during the densification process. Optical microscopy images of through thickness reinforced joints reveal a fully dense core of fill glass surrounded by a fully dense shell of E-glass as depicted in Figures 6 and 7. The index of refraction of soda lime glass and E-glass is sufficiently different such that the interface between the two glasses is readily visible under optical microscopy, as shown in Figure 7.

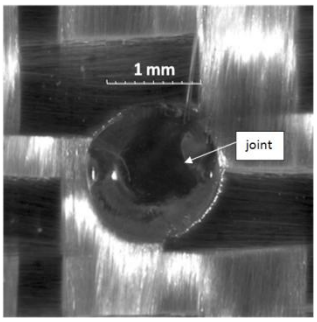

Figure 6: Optical micrograph of a through thickness joint with fill. Note that the center of the joint is fully dense glass with little to no porosity, relatively more transparent than the surrounding fabric.

Similar to the fiber compaction process, laser absorption of the focal volume beneath the fill bead is

induced by the multiple scattering of near-infra red radiation at the numerous fiber interfaces in the fabric. The absorption of the fabric diminishes as fibers compact into a dense joint, and laser energy is able to penetrate further as the fibers coalesce and the number of surfaces is reduced. Laser absorption in the joint is thus self limiting. As dense fill material penetrates through all layers of fabric, the heat into the system is reduced and a steady state condition is achieved when the heat conduction, heat input and viscous resistance to flow are balanced.

Compaction and flow of the fabric material allows for the added glass fill to flow into the E-glass melt, thereby replacing the initial void volume fraction of the fabric. As the laser energy penetrates deeper into the fabric, the fill material also flows deeper into the fabric. The overall morphology of the joint is thereby limited by the initial geometry of the fill material. Glass beads used in this study were selected for their closely matching diameter with the laser spot size.

Fill material in the form of 1mm diameter beads is sufficient to form a continuous joint of up to eight fabric layers in depth (approximately 1.2 mm). Joining of fewer than 8 layers of fabric may also be formed with this process, with a larger joint diameter to accommodate the excess material. Joints in excess of 8 layers showed incomplete melt penetration and reduced fiber connectivity beyond the eight layers. Fabric packing density played an important role in the penetration process, requiring mechanical pressure to be applied on the fabric in order to ensure fill penetration through multiple successive layers. Joint cross sections (Figure 7) show that the joint diameter remains relatively uniform in the through thickness and that there is good fiber to joint connectivity in each layer of the fabric.

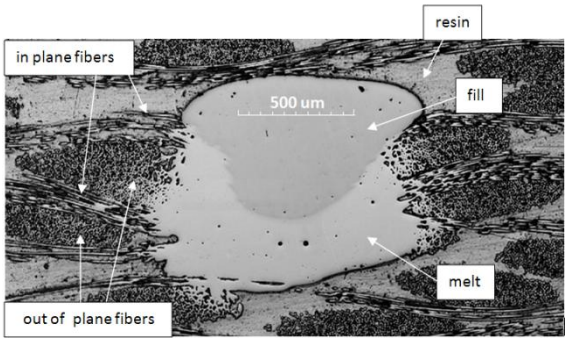

Figure 7: Cross section optical micrograph taken of a four layer through thickness joint cross section. Note that the joint is mostly dense with little to no porosity in the through thickness. The Soda Lime fill glass is observable in optical images from the contrasting index of refraction from the E-glass fiber melt.

Numerical simulations of the fill induced joining process are carried out in the same modeling scheme as presented in the fibrous compaction process. The morphology and temperature evolution during the fill induced joining process are plotted in Figure 8. It is apparent in Figures 7 and 8 that the melt morphology obtained numerically concurs with that obtained from joint cross sections. It is observed from the density and temperature fields produced in the simulation that the flow field during the joining process is consistent with the viscosity gradient and localized heating of the material.

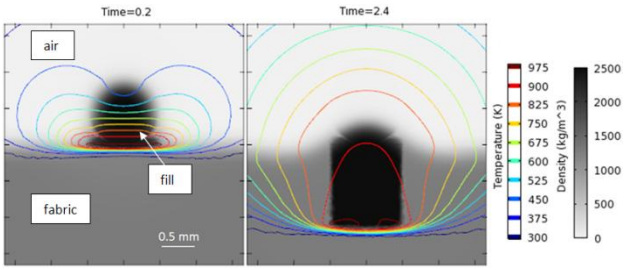

Figure 8: Numerical simulation snap shots of fill induced joining showing the time dependent evolution of the melt morphology during laser fusion joining. Void formation in the substrate is observed to be suppressed by the addition of the fill material. The temperature and morphology of the joint is otherwise shown to be unchanged from the non fill simulation.

Joint Strength

Double cantilever beam (DCB) bending tests of woven fabric composite samples joined in the mid plane, as depicted in Figure 9, have been performed. Fracture energy results from DCB testing show a clear increase in delamination resistance due to joining. During DCB fracture testing, a joined sample exhibits observable start stop crack propagation as the crack front approaches and passes each joint location. Fiber fracture at each joint is detectable in the form of audible snaps as the crack front deflects around the joint and fractures the fibers at the joint interface. Discontinuous start stop crack propagation behaviour was observed during DCB testing and recorded in the load displacement and load crack length output of the MTS system. Fracture toughness, calculated from these results, clearly shows the effect of joining in Figure 10. The discontinuous loading curve observed in joined samples differs dramatically from the relatively smooth fracture process observed in non joined samples, also in Figure 10.

In contrast to joined samples, delamination is observed to occur along the mid plane at a steady rate in all non joined samples. Joined samples resisted the

delaminating crack at each successive joint location until sufficient stresses develop within the beam to break through the joint and propagate forward. Stresses accumulated in the beams during the crack resistance phase are sufficient to rapidly propagate the delamination crack through the composite until it is arrested at the next crack. When a joint fails, a rapid succession of fiber fractures releases a significant amount of built up potential energy in the beams. Visual observation of the fracture process is characterized by the rapid propagation of the crack between joints and extended durations of loading without crack propagation at each joint.

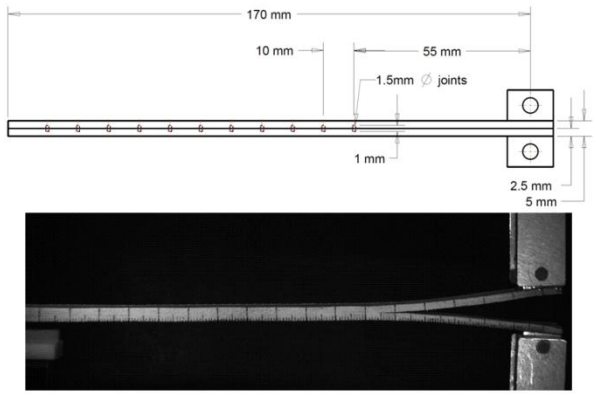

Figure 9: Sample schematic of a laser joined DCB specimen and still image of DCB test during displacement controlled loading. Synchronized capturing of high resolution DCB fracture images enables the calculation of fracture energy with high spatial resolution.

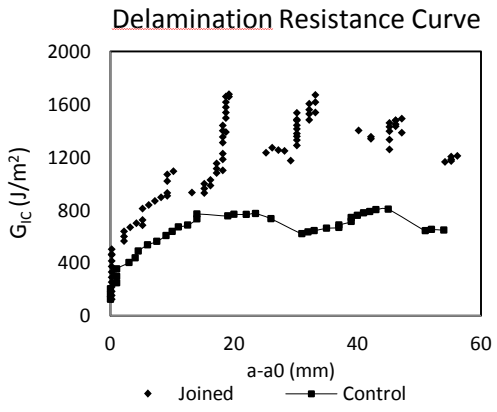

Figure 10: Characteristic DCB fracture energy showing significantly higher fracture energy at joint locations corresponding to the discontinuous load profile observed in the load versus crack length output.

Average fracture energies calculated from DCB tests are plotted in Figure 11. It is apparent from these figures that there exists a positive monotonic relationship between joint thickness and fracture energy. The increased average fracture energy in these tests is clearly a result of the increased peak fracture energies at each joint. Joint fracture energy is a function of the number of crack bridging fibers and as the joint thickness is increased, the total number of fibers fractured per joint is increased. Planar reinforcement density of all samples tested is constant with respect to joint thickness, with joined samples overall exhibiting higher fracture toughness than non-joined samples. The clearly separate fracture energies obtained from this study indicates that with a higher planar density of joints, the average fracture energy of the sample will increase due increased frequencies of peak fracture toughness. Experimental evidence of fiber fracture at the joint interface is observed in scanning electron microscopy images of the fracture surfacee.

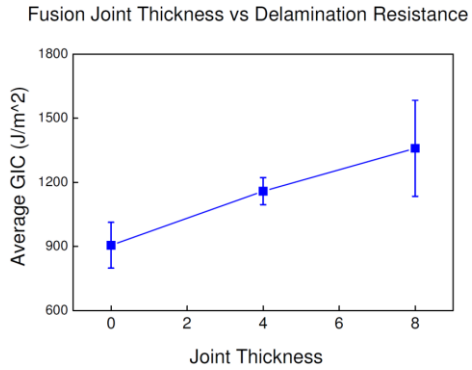

Figure 11: Compiled data of the average DCB fracture energy as a function of joint thickness. Note that the average fracture energy follows an approximately linear trend with the joint thickness due to the higher maximum load and peak fracture energies exhibited at the joint locations.

Fracture Surface Morphology

Examination of the fiber fracture surfaces under SEM shows a large density of fiber fractures at the leading edge of joints as opposed to non-joined areas. Contrasting fracture surfaces between joined regions of post mortem DCB samples are shown in Figure 13. Fracture between layers of reinforcement is observed to take place at the fiber/matrix interface, leaving an undulating surface profile characteristic of the woven fiber structure. Little to no fiber fracture is observed in these regions with characteristic brittle fracture of the matrix phase. In contrast to the surface profile observed at non joined regions, the fracture pattern around joints is characterized by large amounts of fiber fracture and significant out of plane crack deflection. It is observed in Figure 13 that crack deflection and

fiber fracture effects lead to a positive and negative feature of the joint protruding from the relatively flat fracture surface around it. The effect of crack deflection is also observed in the branching of multiple cracks to adjacent layers of fabric, as is observed during DCB testing. SEM images of the joint surface after testing clearly show a high density of fiber fractures at the surface of the joints (Figure 14). Fiber fracture and crack branching are two key mechanisms of the increase in fracture toughness observed in laser joined samples.

It is observed that joint failure tended to occur during the rapid energy release from a highly loaded location. Rapid crack propagation is observed to occur once the elastic stress within the beam is suddenly released after an extended stop at a particular joint. Rapid crack propagation through the non-joined surfaces between laser treated regions would on some occasions lead to the fracture of the following joint rather than the desired fiber fracture behavior. Through thickness joint strength, as defined by Griffith's criteria, is characterized by the critical flaw size of the joint. It is expected that reducing the diameter of the joint will increase its critical load, allowing for greater peak fracture energies and increased delamination resistance.

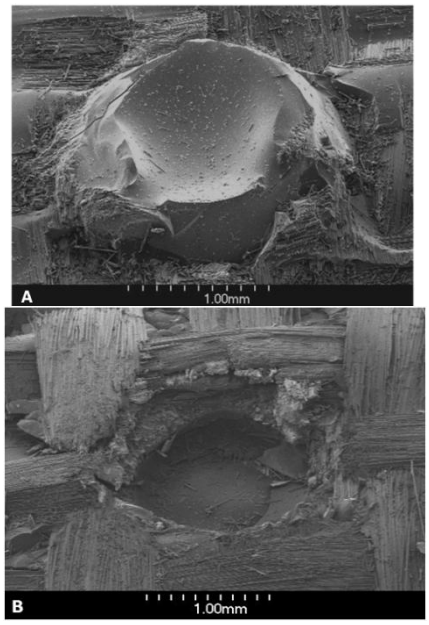

Figure 12: SEM images of joint fracture surfaces showing fiber fracture and crack branching behavior due to crack deflection at joints. A positive and negative imprint of the joint remains after the crack has propagated around the joint.

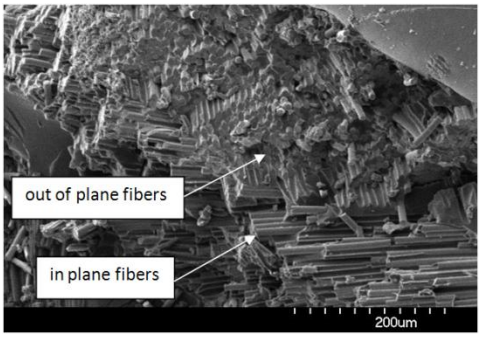

Figure 13: SEM image of fiber fracture surfaces around a single joint. Fibers from multiple layers are observed from the cross ply orientations of the fracture surfaces.

Conclusions

A fusion joining method has been developed to selectively reinforce glass fiber composites in the through thickness direction. Fiber compaction, densification and flow effects have been simulated using a multi physics numerical solver modeling the viscous flow, densification and heat dissipation effects of glass fabric during the fusion process. Numerical predictions of joint diameter and depth have been validated with measurements of fabric melt morphology observed under optical microscopy.

Mechanical testing of fusion joined samples has shown an increase in mode one fracture toughness as a function of the joint penetration thickness. Toughening effects of inter laminar joining is clearly observable in delamination resistance curves. Scanning electron microscopy images of the fracture surface show significant crack blunting and deflection at each of the joints, corresponding to the experimentally observed increase in local fracture toughness.

Through thickness reinforcement of woven glass fiber composites has been shown to be a viable laser fusion process. Findings from the experimental evaluation of fracture toughness indicate significantly increased delamination resistance as a function of joint thickness and area density. The application of fusion joints in areas of high inter laminar stress concentrations is proposed as a flexible and effective method to mitigate the onset of composite delamination.

Acknowledgements

The use of material testing equipment and synchronized imaging system was provided by the Soft Tissue Biomechanics lab thanks to Dr. Kristin Meyers and Kyoko Yoshida. Partial financial support from Columbia University is gratefully acknowledged.

References

[1] Byrd L., and Birman V., 2006, "Effectiveness of z-pins in preventing delamination of co-cured composite joints on the example of a double cantilever test," Composites Part B: Engineering, **37**(4-5), pp. 365-378.

[2] Bilisik K., 2009, "Multiaxis 3d woven preform and properties of multaxis 3d woven and 3d orthogonal woven carbon/epoxy composites," Journal of Reinforced Plastics and Composites, **29**(8), pp. 1173-1186.

[3] Bogdanovich A. E., 2006, "Advancements in manufacturing and applications of 3-d woven preforms and composites," 16th international conference on composite materials, pp. 1-10.

[4] Mohamed M. H., and Wetzel K. K., 2006, "3D woven carbon/glass hybrid spar cap for wind turbine rotor blade," Journal of Solar Energy Engineering, **128**(4), p. 562.

[5] Niebel V., Weinert N., Gries T., and Seliger G., 2009, "Technology for overlap-free joining of semi-finished textile products," Technical Textiles, **52**(2), pp. E68-69.

[6] Jones I., 2005, "Improving productivity and quality with laser seaming of fabrics," Technical Textiles International, (May), pp. 35-38.

[7] Rahaman M. N., Jonghe L. C. De, Scherer G. W., and Brook R. J., 1987, "Creep and Densification During Sintering of Glass Powder Compacts," Journal of the American Ceramic Society, **70**(10), pp. 766-774.

[8] 2007, "Standard Test Method for Mode I Interlaminar Fracture Toughness of Unidirectional Fiber-Reinforced Polymer Matrix Composites 1," Annual Book of ASTM Standards, pp. 1-12.

[9] Chen J. C., and Churchill S. W., 1963, "Radiant heat transfer in packed beds," AIChE Journal, **9**(1), pp. 35-41.

[10] Sun W., Loeb N. G., and Fu Q., 2002, "Finite-difference time-domain solution of light scattering and absorption by particles in an absorbing medium," Applied Optics, **41**(27), pp. 5728-5743.

[11] Kask N. E., Radchenko V. V., Fedorov G. M., and Chopornyak D. B., 1979, "Temperature dependence of the absorption coefficient of optical glasses exposed to laser radiation," Nuclear Physics, **9**(2), pp. 193-198.

[12] Gardon R., 1954, "Review of radiant heat transfer in glass," Journal of the American Ceramic Society, **44**(7), pp. 305-312.

[13] Dvurechensky A. V., Petrov V. A., and Reznik V. Y., 1979, "Spectral emissivity and absorption coefficient of silica glass at extremely high temperatures in the semitransparent region," Infrared Physics, **19**, pp. 465-469.

[14] Kuczynski G. C., 1949, "Study of the sintering of glass," Journal of Applied Physics, **20**(12), pp. 1160-1163.

[15] Kingery W. D., and Berg M., 1951, "Study of the Initial Stages of Sintering Solids by Viscous Flow, Evaporation-Condensation, and Self-Diffusion," Journal of Applied Physics, **3**, pp. 1205-1212.

[16] Smiley a. J., and Pipes R. B., 1987, "Rate Effects on Mode I Interlaminar Fracture Toughness in Composite Materials," Journal of Composite Materials, **21**(7), pp. 670-687.

[17] Tan H., and La Y., 2012, "Laser Joining of Continuous Glass Fiber Composite Pre-forms," Journal of Manufacturing Science and Engineering. Under Review

[18] Fluegel A., 2007, "Glass viscosity calculation based on a global statistical modelling approach," Glass Science And Technology, **48**(1), pp. 13-30.

[19] Kolossov S., Boillat E., Glardon R., Fischer P., and Locher M., 2004, "3D FE simulation for temperature evolution in the selective laser sintering process," International Journal of Machine Tools and Manufacture, **44**(2-3), pp. 117-123.

[20] Hopper R. W., 1993, "Coalescence of Two Viscous Cylinders by Capillarity: Part 1, Theory," J. Am. Ceram. Soc., **76**(12), pp. 2947-52.

[21] Scherer G. W., 1991, "cell models for viscous sintering," Journal of the American Ceramic Society, **74**(7), pp. 1523-1531.

[22] Mackenzie J. K., and Shuttleworth R., 1949, "A Phenomenological Theory of Sintering," Proceedings of the Physical Society. Section B, **62**(12), pp. 833-852.

[23] Tempel L. V. D., 2002, "Thermal Conductivity of a Glass: II . The Empirical Model," **28**(3), pp. 147-152.

[24] Grove F. J., 1961, "Spectral Transmission of Glass at High Temperatures and Its Application to Heat-Transfer Problems," Journal of the American Ceramic Society, **44**(7), pp. 1956-1959.

[25] Condon E. U., 1968, "Radiative Transport in Hot Glass," Journal of Quantitative Spectroscopy and Radiative Transfer, **8**, pp. 369-385.